Mon. Not. R. Astron. Soc. **000**, 1–?? (0000) Printed 31 January 2000 (MN LaTeX style file v1.4)

A photometric study of the eclipsing symbiotic binary AR Pavonis

A. Skopal[1,2⋆], G. Djurašević[3], A. Jones[4], H. Drechsel[1], H. Rovithis-Livaniou[5], P. Rovithis[6]

[1]*Astronomisches Institut der Universität Erlangen-Nürnberg, Sternwartstr. 7, D-96049 Bamberg, Germany*
[2]*Astronomický ústav Slovenskej akadémie vied, SK-05960 Tatranská Lomnica, Slovakia*
[3]*Astronomical Observatory, Volgina 7, 11050 Belgrade, Yugoslavia*
[4]*Carter Observatory, P.O. Box 2909, Wellington 1, New Zealand*
[5]*Section of Astrophysics, Astronomy and Mechanics, Department of Physics, University of Athens, 157 83 Athens, Greece*
[6]*Astronomical Institute, National Observatory of Athens, 118 10 Athens, Greece*

Received; in original form

ABSTRACT

In this study we present and re-analyze the historical, 1889 – 1998, light curve (LC) of the eclipsing symbiotic binary AR Pav. For the first time, we showed that timing of mid-points of eclipses observed during a quiescent phase obeys a quadratic ephemeris, with an initial orbital period $P_0 = 605.18$ days and a rate of period change $\dot{P} = -3.5 \pm 0.8 \times 10^{-5}$.

We determined a distance to the system of 5.8 ± 1.5 kpc, the mass ratio of the giant to the hot star, $M_{\rm g}/M_{\rm h} = 0.4 \pm 0.1$, the mass of the giant, $M_{\rm g} = 1.8 + 1/-0.5\,{\rm M}_{\odot}$ and its radius, $R_{\rm g} = 167 \pm 15\,{\rm R}_{\odot}$.

During quiescence, the LC has characteristic features similar to those observed in cataclysmic variables (CVs). It can be well reproduced by a model of a large accretion disk surrounding the hot star. However, it is probable that the geometry of the transferred material in the Roche lobe of the accretor in AR Pav is different from that of CVs.

During active phases the shape of the LC changes considerably. A complex wave-like variation developed as a function of the orbital phase with an amplitude of $\sim$1 mag. It is interpreted in terms of a collisionally heated emission region located on the giant surface due to the hot star eruption.

Key words: binaries: eclipsing – binaries: symbiotics – stars: fundamental parameters – stars: individual: AR Pav

1 INTRODUCTION

AR Pav is a well-known eclipsing symbiotic binary with an orbital period of 605 days (Mayall 1937). It consists of a cool M3-4(III-II) giant (Schulte-Ladbeck 1988) filling its Roche lobe and losing mass to an evolved, $\sim$30 000 K hot, compact object surrounded by a moderately dense gas cloud or a thick ring (Thackeray 1959; Thackeray & Hutchings 1974). Fitting the *UV* continuum by a synthetic spectrum, Kenyon & Webbink (1984) revised this model arguing for the presence of an accretion disk around a main sequence star. The eclipsed object is highly variable in both brightness and size (e.g. Andrews 1974). On the basis of ultraviolet spectroscopy Hutchings et al. (1983) confirmed this view and showed that the eclipses must be at least partially of an extended region, and not simply of the hot star. From 1985.7, Bruch, Niehues & Jones (1994) observed a periodic ($\sim P_{\rm orb}$) wave-like variation in the visual LC which occurred between eclipses. They conclude that such behaviour is not easily explained by the present models.

In this contribution we re-analyze the historical LC of AR Pav. In Sect. 2 we describe its basic observational characteristics and in Sect. 3 we derive some fundamental parameters of the system and discuss processes of interaction in AR Pav.

2 OBSERVATIONS

Our study of AR Pav is based on historical photometric measurements recorded from 1889 to the present time. There are two large data sets: (i) the 900 photographic magnitudes of Mayall (1937) covering the period 1889 to 1936.5 and (ii) about 2300 visual magnitude estimates made by one of us (AJ) during 1982 to 1999. In addition, we use photoelectric observations of Andrews (1974), Menzies et al. (1982) and the data measured by Kohoutek (1999) from photographic plates collected in the archive of the Bamberg Observatory.

⋆ Visiting Astronomer, University of Athens

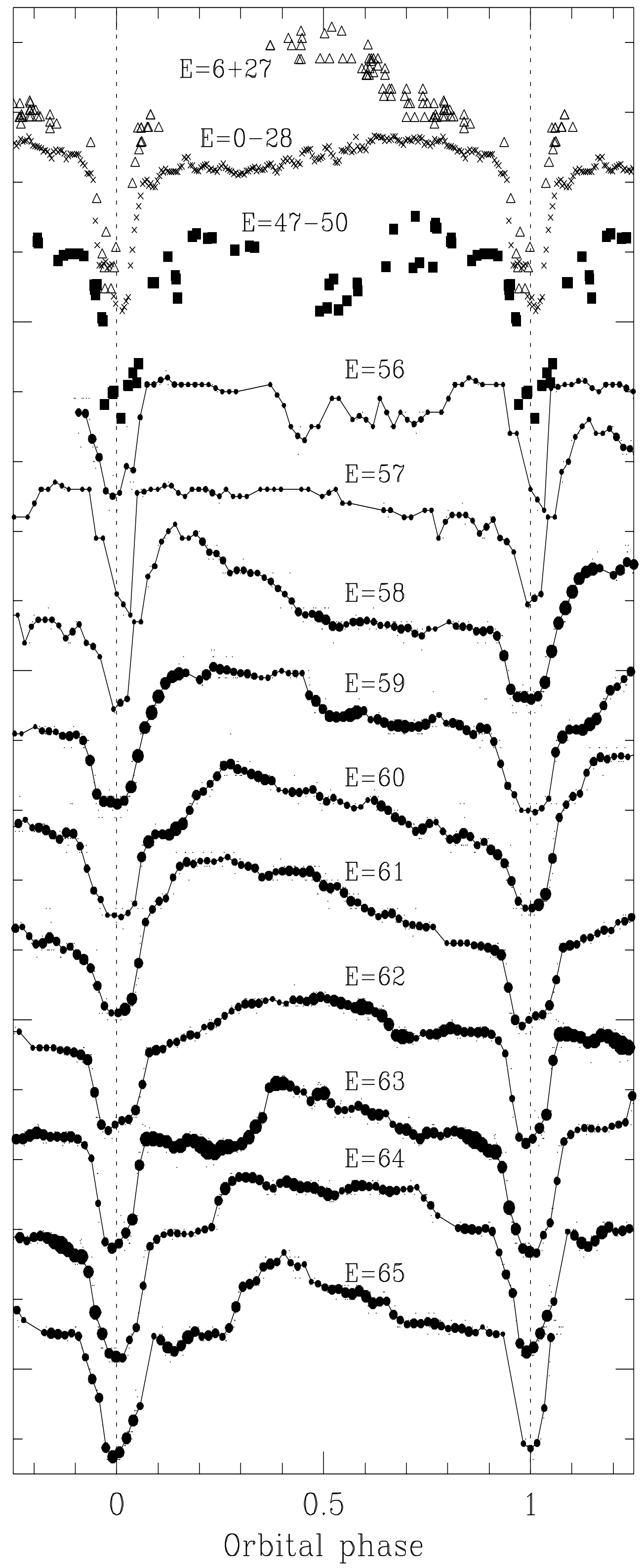

Figure 1. Historical LC of AR Pav. It consists of the photographic data published by Mayall (1937) (epochs 0 to 28), photoelectric *V* data of Andrews (1974) (47-50), and visual estimates (dots) made by one of us (A.J.) (56-65). Full circles represent smoothed data in 20-day bins, and their size corresponds to a weight from 1 to 20. Data sets are shifted by 1.5 mag relative to each other, and the ticks are separated by 1 mag.

2.1 Evolution in the light curve

Figure 1 shows the historical LC of AR Pav. Its individual cycles are folded with the ephemeris (1). Variability in the LC has already been reported by Mayall (1937). Andrews (1974) discussed a significant change in the minimum profile and its position during the outburst at the epoch E=6 caused by an increase of the hot component size. Bruch et al. (1994) noted that individual eclipses, observed during the recent activity (from $\sim$ 1986), differ in both shape and width. They observed a strong wave-like behaviour at a level of $\sim$1 mag, which developed between eclipses from 1986 on.

In adition to the known variation in the LC of AR Pav we found a periodic brightness fluctuation in the visual band. We used the data out of eclipses, during cycles E = 58, 59, 63 and 65, where the variability is more pronounced. After subtracting the out-of-eclipse behaviour we found a period of 106.4 days by using a phase dispersion minimization method and Fourier analysis. We did not find this type of variation in the photographic observations. Figure 2 shows the phase diagram of the used data folded with the period $P_{\rm obs}$ = 106.4 days. The average points represent means in $0.1\times P_{\rm obs}$ bins with a $0.05\times P_{\rm obs}$ step width. The amplitude of this variation is about 0.15 mag. The uncertainty of average points, 0.03 to 0.04 mag, results from the uncertainty of individual estimates, 0.3 to 0.4 mag, and the number of data in the 10.64-day bins being about 80 to 100. However, due to a lower significance of the 106.4-day period in the visual data (θ=0.9; power=0.002), its independent confirmation by infrared photometry is needed.

Finally, from the contact times of the available minima we derived the evolution of radii of the eclipsed object and the giant star (Figs. 3, 4).

2.1.1 *Quiescent phase*

First we treated Mayall's photographic data. We subtracted a long-term variation in the LC by a polynomial fit and smoothed the data by a filter of width 0.025 $P_{\rm orb}$ with a step of size 0.005 $P_{\rm orb}$. Then we folded the data using the ephemeris (1) into a phase diagram (Figs. 1 top and 8). In such a phase representation we can easily distinguish a quiescent phase from outbursts. During the period of these observations (1889-1936), AR Pav remained in quiescence most of the time. There are two most significant features in the quiescent LC: (i) a bump of extra light arising from phase $\sim$ 0.4 and causing that the brightness after eclipses remained $\sim$ 0.5 mag fainter than before it; (ii) a standstill just before the minimum (at $\varphi \sim 0.97$). We note that these characteristics are also clearly seen in Fig. 2 of Mayall (1937). Generally, the LC has a characteristic shape similar to the LCs of dwarf novae in quiescent phase. This similarity suggests an intense exchange of material between the components. In Sect. 3.4 we discuss the LC in more detail.

A significant change in the LC profile was measured by Andrews (1974) from 1967 to 1973 (cycles 47 to 50). His *UBV* LCs cover a quiescent phase only, and the profile lost the two main signatures apparent in Mayall's LC. In addition, it displays an about 0.3 $P_{\rm orb}$ broad and $\sim$1 mag deep secondary minimum in all bands, and the profile varies from cycle to cycle (cf. Fig. 1 of Andrews (1974); also Fig. 1 top here). This drastic change is probably connected with the creation of a large nebulosity around the hot star during that time. Its presence is indicated by highly negative values of the $U-B$ index. The broad secondary minimum could result from the projection of the optically thick portion of an asymmetrical HII zone into the line of sight (see Skopal 1998 for more details). Contribution of the nebular component of radiation varies

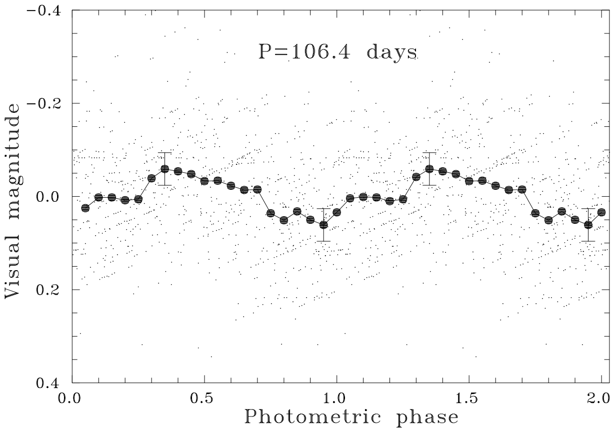

Figure 2. Variability in the visual band indicating a period $P_{\rm obs}$=106.4 days. The full points represent means of all individual estimates in 0.1 $P_{\rm obs}$ bins made with 0.05 $P_{\rm obs}$ step width.

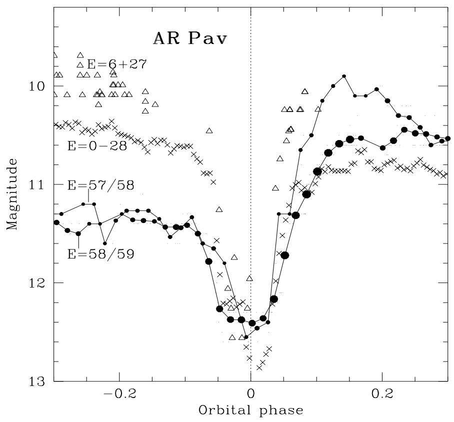

Figure 3. Comparison of the minima profiles in different epochs. Denotation of the data as in Fig. 1. Note a relatively stable profile of eclipses during 28 orbital cycles of the 1889–1936.5 quiescence in contrast to rapid changes between individual cycles during the recent activity.

during different epochs. For example, Bruch et al. (1994) measered considerably redder radiation in eclipses at E = 58 and 61 than Andrews (1974) at E = 47 – 50.

During quiescence, the radius of the eclipsed object was relatively stable, being of $\sim 0.1A$, where A stands for the separation between the stars (Fg. 4).

2.1.2 Active phases

In 1900 and 1935 AR Pav underwent two outbursts lasting about one orbital period. The corresponding LC is strongly phase dependent. It displays a wave-like modulation along the orbital cycle with maximum light around orbital phase 0.5, i.e. when the hot component is in front (Fig. 1 top, Fig. 8). The amplitude is about 1.5 mag. Such phase-dependent brightness variation developed also during outbursts of AX Per (cf. Skopal 1994 – hereafter S94).

The LC recorded from 1982 to the present (cycles 56 to 65) again reflects significant variations. From 1985.7 (E=58) AR Pav has started an active stage. An extra and variable light has developed between eclipses. At the beginning of this activity maxima occurred shortly after eclipses ($\sim$100 days) followed by a slower decline to the next eclipse. Later, from cycle 62 on, a sudden rise to maximum occurs after a 0.2–0.3 $P_{\rm orb}$ lasting plateau from eclipse, closer to orbital phase 0.5 (cf. Fig. 1). In spite of these complex features, the basic characteristics of this out-of-eclipse variation resemble those observed in 1900 and 1935 outbursts.

During active phases we also observe a strong variation of the eclipsed light source. Figures 1, 3 and 4 suggest that the source of the optical light, which is subject to eclipse, is very unstable during the recent activity. As a result the position of minima changes considerably (Sect. 3.1 below).

3 ANALYSIS

3.1 Ephemeris and period change

Mayall (1937) derived from her data photometric elements for AR Pav as

$$\mathrm{Min(pg)} = \mathrm{JD}\,2\,411\,255{+}605{\times}E.$$

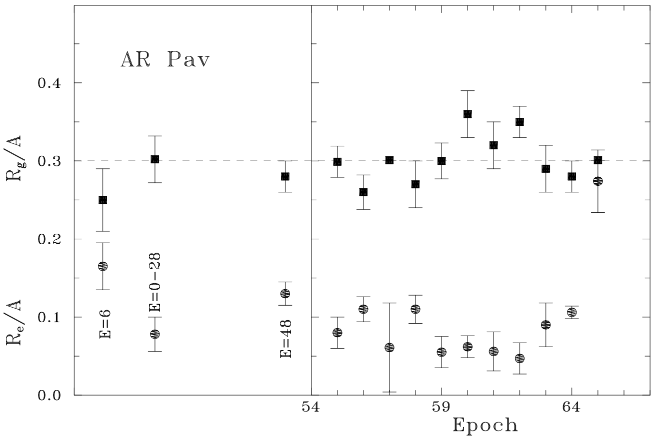

Figure 4. Variation of radii of the giant star and the eclipsed object. The minimum at E = 65 is characterized by broad wings indicating a significant extent of the eclipsed object.

Andrews (1974) made a new determination from his and Mayall's data as

$$\mathrm{Min} = \mathrm{JD}\,2\,420\,330{+}604.6{\times}E.$$

Finally, Bruch et al. (1994) refined it to

$$\mathrm{Min} = \mathrm{JD}\,2\,420\,331.3{+}604.5{\times}E,$$

based on Mayall's, Andrews', Menzies et al. (1982), and the present visual observations between 1982 and 1993. The above mentioned ephemerides suggest a decreasing trend in the orbital period. Therefore, and for reasons described in Sect. 2.1, we re-analyzed the historical LC using a standard $O-C$ method to verify this view.

First, we determined positions of eclipses for which there are sufficient data. We employed several methods with respect to the shape and data coverage of the minima. Particularly we used the method of a parabola fit, Kwee and Van Woerden's method, sliding integration method, trace paper method, polygonal line method and "center of mass" method, which are described in detail by Ghedini (1982). Resulting positions of eclipses are listed in Table 1. They represent average values from those obtained by different methods, which usually coincided within their uncertainties. As the resulting uncertainty in the position of the minima we adopted that deter-

Table 1. Observed mid-points of eclipses and their $O-C$ residuals from the linear ephemeris (1)

E	$\mathrm{JD_{Min}}(O)$	I	$\mathrm{JD_{Min}}(C)$	$O-C$	Method[a]
4	2413678.4± 1.9	7	2413683.7	-5.3	1,2,3,4,5,6
6[b]	14881.3± 1.5	10	14892.6	-11.4	1,2,4,5,6
9	16705.3± 2.3	9	16706.0	-0.7	1,2,3,4,5,6
12	18519.0± 3.8	6	18519.4	-0.4	1,2,4,5,6
15	20333.4± 3.6	9	20332.8	0.6	1,2,3,4,5,6
21	23960.6± 2.0	10	23959.5	1.1	1,3,4,6
24	25776.2± 3.0	7	25772.9	3.3	1,2,3,4,6
27	27589.5± 1.0	13	27586.2	3.3	1,2,3,4,6
47[c]	39679.1± 1.7	15	39675.3	3.8	1,3,4,6
50[d]	41492.0		41488.7	3.3	
56	45113.7± 2.0	19	45115.4	-1.7	1,2,4,5,6
57	45718.7± 2.3	5	45719.9	-1.2	1,4
58	46321.4± 2.2	11	46324.4	-3.0	1,4,6
59	46924.7± 0.4	44	46928.8	-4.1	1,3,5,6
60	47531.7± 0.9	18	47533.3	-1.6	1,2,3,4,6
61	48138.1± 0.5	30	48137.7	0.4	1,2,4,5,6
62	48742.6± 0.6	34	48742.2	0.4	1,4,5,6
63	49347.8± 0.6	30	49346.6	1.2	1,2,4,5,6
64	49951.8± 0.5	41	49951.1	0.7	1,3,4,5,6
65	50555.5± 0.8	36	50555.5	0.0	1,3,4,5,6

a: 1 - parabola fit, 2 - Kwee and van Woerden method, 3 - sliding integration method, 4 - tracing paper method, 5 - polygonal line method, 6 - "mass center" method.
b: this minimum was not used in our determination of ephemerides.
c: according to Kohoutek (1999)
d: after Andrews (1974)
I - number of available data defining the minimum.

mined by the sliding integration method and Kwee and van Woerden method, and in some cases (E = 12, 21, 58, 60) also from the parabola fit. The minimum at epoch E=6 was not used for our analysis. It is shifted by about -11 days with respect to the other minima due to the eruption of the active component (see Andrews 1974).

Second, with respect to the significant difference in the eclipse profiles between the phases of quiescence and activity (Sect. 2.1), we distinguished in our analysis two data sets: (i) the minima measured in the quiescent LC, i.e. at epochs E = 4–58 (except that at E = 6 which is corrupted by the outburst), and (ii) the minima observed during the recent activity, i.e. E = 59–65. We also determined an average ephemeris from all the minima and compared it with the cases (i) and (ii). Results of our analysis are summarized in Table 2 and plotted in Fig. 5.

Linear regression through all the observed mid-points of eclipses (without E = 6) yields their timing as

$$\mathrm{Min} = \mathrm{JD}\,2411265.9 + 604.46(\pm 0.02) \times E, \tag{1}$$

which is (nearly) identical with that derived by Bruch et al. (1994). The uncertainty in the period was determined in a standard way (e.g. Batten 1973) for an average error in individual positions of 2-3 days. However, the residuals from it (Table 1, panel 1 of Fig. 5) display a parabolic shape. A parabola fit throughout all data makes the quantity of χ^2 $(=\Sigma(O-C)^2/\mathrm{N}$, where N is the number of minima used) smaller by a factor of 1.7, but it is unsatisfactory for the eclipses at E = 59–65, positions of which are determined with an accuracy of about ±0.7 days. As a result we analysed the data during quiescence (E = 4–58) separately. The linear fit to them (No. 3 in Table 2) gives the largest χ^2 and yet more pronounced parabolic shape of its residuals (panel 3 in Fig. 5). Contrary, the parabolic fit to these eclipses provides the smallest value of χ^2 (No. 4 in Table 2) and residuals from it are scattered around zero within their uncertainties (panel 4 of Fig. 5). Finally, the ephemerides derived from eclipses of a relatively short interval of the recent AR Pav activity (No. 5 and 6 in Table 2) suggest an abrupt change in the period. However, this probably results from a significant variation of the eclipse profiles during the present active phase (Sect. 2.1), which is not connected with the orbital motion of the binary components. On the other hand, a continuous (parabolic) variation in the $O-C$ values from their linear fit (panel 5 of Fig. 5) reflects a regular change in the eclipse positions due to a process being in effect throughout the whole activity.

As a result of this analysis we suggest to use the average linear ephemeris (1) to estimate the position of forthcoming minima (e.g. for scheduling observations). However, timing of the eclipses during the long-term quiescent phase between epochs 4 and 58 shows a regular parabolic variation, which can be interpreted in terms of

Table 2. Possible ephemerides for the observed minima

No.	Epochs	$\mathrm{JD_0}$	Period		χ^2
		Linear fit			
1	4–65	2 411 265.9	604.46		5.92
3	4–58	2 411 265.7	604.47		7.41
5	59–65	2 411 226.7	605.08		1.32
		Parabolic fit			
No.	Epochs	$\mathrm{JD_0}$	$\mathrm{A_1}$	$\mathrm{A_2}$	χ^2
2	4–65	2 411 260.8	604.89	-0.0061	3.43
4	4–58	2 411 258.2	605.17	-0.0107	0.94
6	59–65	2 409 987.8	645.08	-0.3226	0.07

Meaning of parameters $\mathrm{A_1}$ and $\mathrm{A_2}$ is given by Eq. (2).

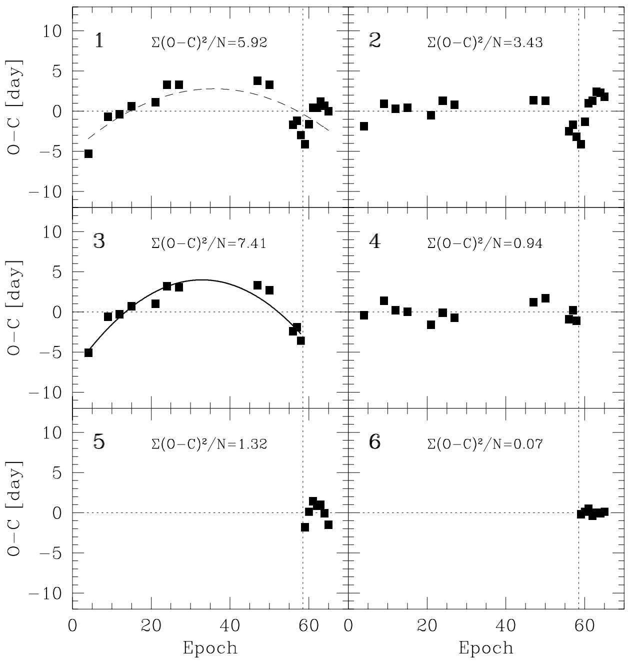

Figure 5. Residuals resulting from linear (left panels) and parabolic (right panels) ephemerides listed in Table 2. The numbers of panels correspond to the numbers of ephemerides in Table 2.

a real change – a continuous decrease – of the orbital period of the binary. We derive basic properties of this parabolic ephemeris (No. 4 in Table 2), the initial period P_0 and the rate of period change $\dot{P}$. For the case of a continuous change in the period by $\dot{P} = \Delta P/P$ we derived the quadratic ephemeris for timings of the minima as

$$\mathrm{Min} = JD_0 + (P_0 + \frac{1}{2}P_0\dot{P}) \times E + \frac{1}{2}P_0\dot{P} \times E^2. \qquad (2)$$

Comparing it to our calculated ephemeris (No. 4 in Table 2), we found the rate of change of the period to be

$$\dot{P} = -3.5 \pm 0.8 \times 10^{-5} \quad (= 1.3 \text{ days per } 100 \text{ years})$$

and an initial orbital period P_0 = 605.18 days.

The rate of change of the orbital period is often used for determination of the mass transfer between the components of an interacting binary. In the most simple case in which mass and angular momentum are conserved, the orbital period can decrease only, if mass is being transferred from the more to the less massive component. This conservative approach is evidently unsatisfactory for AR Pav as its donator is the less massive star (Sect. 3.2 below). A steadily shorter orbital period can be produced, for example, by a 'slow' mass and angular momentum loss from the binary. In AR Pav we have a direct indication of such an outflow through the P-Cygni type of profiles of hydrogen lines with a strong shortward shifted absorption (Mayall 1937; Thackeray 1959; Thackeray & Hutchings 1974). However, we do not know the precise way in which the mass is ejected, which determines the angular momentum loss from the system. Therefore we leave this complex problem open for furher investigation.

3.2 Radii and masses of the components

Andrews (1974) estimated the radii of the components in AR Pav to be $0.35A$ and $0.15A$ for the cool and hot star, respectively. Thackeray & Hutchings (1974) derived a mass function of $0.14\,\mathrm{M}_\odot$ for the hot star and suggested masses of order 2.5 and $1.2\,\mathrm{M}_\odot$ for the hot and cool star as most likely, assuming the mass ratio $q = M_\mathrm{g}/M_\mathrm{h}$ = 0.5. Recently Bruch et al. (1994) derived a mean eclipse duration of 82±2 days from well defined minima at E = 56, 59, 60 and 62.

Observational results of this paper and those previously published constrain the following limits for radii and masses of the components of AR Pav:

(i) Our analysis of all the available minima (Fig. 4) yields an average radius of the giant, R_g, as

$$R_\mathrm{g}(eclipse) = (0.30 \pm 0.02)A, \qquad (3)$$

where the separation A of the two stars in the binary is defined through Kepler's law as

$$A = \left[\frac{GP^2}{4\pi^2}M_\mathrm{h}(1+q)\right]^{1/3}, \qquad (4)$$

with the mass ratio $q = M_\mathrm{g}/M_\mathrm{h}$.

(ii) From a modeling of the LC (Sect. 3.4.1) and suggestions made by other authors (Thackeray & Hutchings 1974; Andrews 1974; Kenyon & Webbink 1984), the giant in AR Pav fills up its Roche lobe. So, we can write its radius as

$$R_\mathrm{g}(Roche\ lobe) = \left[\frac{3}{4\pi}V_\mathrm{L}(q)\right]^{1/3}, \qquad (5)$$

where $V_\mathrm{L}(q)$ is the Roche lobe volume. We calculated the Roche

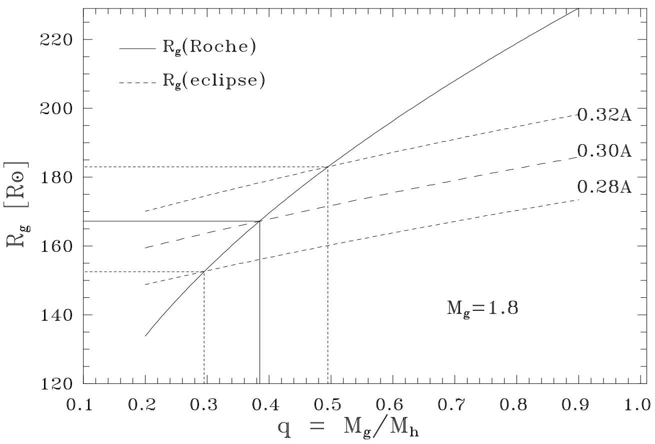

Figure 6. Plots of the red giant radii given by Eqs. (3, 5) as function of the mass ratio q for the mass of the giant star of $1.8\,\mathrm{M}_\odot$, which satisfies the mass function of $0.14\,\mathrm{M}_\odot$ for $i = 90°$.

lobe radius by using our own code RLOBE, which is in a very good agreement with that determined by the Eggleton's (1983) formula. The radii determined by Eqs. 3 and 5 are equivalent for

$$q = 0.4 \pm 0.1,$$

(see Fig. 6) for arbitrary values of the hot component mass. Then the mass function for the hot star, $f_\mathrm{h}(m) = 0.14\,\mathrm{M}_\odot$ (Thackeray & Hutchings 1974), defines the mass of the giant as

$$M_\mathrm{g} = 0.14(1+q^{-1})^2 = 1.8 + 1/-0.5\,\mathrm{M}_\odot$$

for the orbital inclination of 90°. The limits here are given by the uncertainty of q. However, they can be even larger, because of a possible uncertainty in the mass function. Finally, relations 3 and 5 for the derived q and the mean value of M_g given above yield a radius

$$R_\mathrm{g} = 167 \pm 15\,\mathrm{R}_\odot.$$

The uncertainty represents that of our estimation from the minima (Eq. 3), see also Fig. 6.

In addition, we tried to verify this result by assuming that the observed periodic variation in the visual LC with $P_\mathrm{obs} \sim$106.4 days is caused by radial pulsations of the red giant. Then the corresponding radius can be found from a period-mass-radius relation. According to Ostlie & Cox (1986), for the fundamental mode, in units of $\mathrm{R}_\odot$, day, $\mathrm{M}_\odot$, we can write

$$\log R_\mathrm{g}(pulsation) = [\log P_\mathrm{obs} + 0.73\log(M_\mathrm{g}) + 1.92]/1.86, \qquad (6)$$

which is valid for masses up to $2.0\,\mathrm{M}_\odot$. For $M_\mathrm{g} = 1.8 + 1/-0.5\,\mathrm{M}_\odot$ we get $R_\mathrm{g}(pulsation) = 167 + 31/-20\,\mathrm{R}_\odot$, which agrees well with the radius determined from relations 3 and 5.

3.3 Distance of AR Pav

Thackeray & Hutchings (1974) based their estimate of the distance on a spectral classification of the giant in AR Pav as M3 with M_V=-0.4. Then for its apparent visual magnitude of 12.5, however, not considering a correction for the interstellar absorption, they obtained the distance d = 3.8 kpc. If we correct the visual magnitude with $E_\mathrm{B-V}$=0.26 (Kenyon & Webbink 1984) we get d=2.6 kpc. Kenyon & Webbink (1984) suggested the distance of AR Pav to be between 4.5 and 5.8 kpc. They assumed a giant's

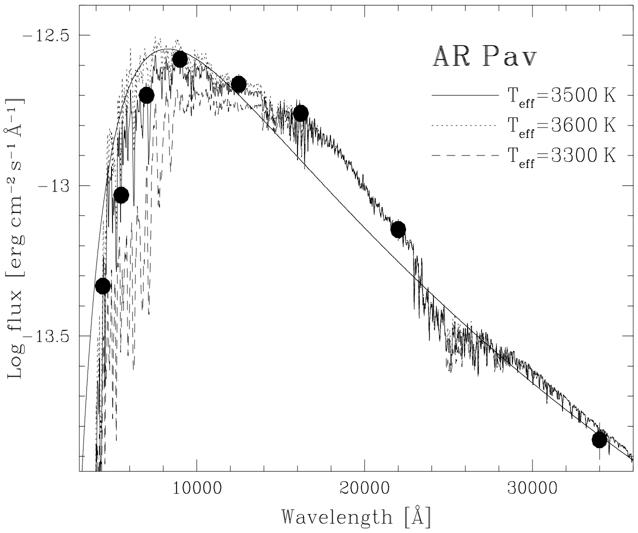

Figure 7. Optical/infrared energy distribution of AR Pav given by the broad band photometry (•). Compared are synthetic spectra of $T_{\rm eff}$ = 3 300, 3 500 and 3 600 K according to Hauschildt (1999a). The full smooth line is the Planckian function for 3 500 K, scaled to the luminosity of the corresponding synthetic spectrum.

radius of $R_{\rm g} = 105\,{\rm R}_{\odot}$ and K=7.16 mag, corresponding to M3 spectral type.

In our approach we tried to estimate the angular diameter of the cool component, $\theta = R_{\rm g}/d$, which for its known radius, $R_{\rm g}$, defines the distance, d. The bolometric luminosiy of the giant can be written as

$$L = 4\pi d^2 F_{\rm g}^{\rm obs} = 4\pi R_{\rm g}^2 F_{\rm g}, \qquad (7)$$

where $F_{\rm g}^{\rm obs}$ refers to flux at the Earth's surface and $F_{\rm g}$ is the emitted flux at the stellar surface. Effective temperature, $T_{\rm eff}$, is defined in terms of the star's luminosity and radius by $L = 4\pi R_{\rm g}^2 \sigma T_{\rm eff}^4$. Thus using Eq. (7) we can express the angular diameter in terms of $T_{\rm eff}$ and $F_{\rm g}^{\rm obs}$ as

$$\theta = \sigma^{-1/2} \left(\frac{F_{\rm g}^{\rm obs}}{T_{\rm eff}^4} \right)^{1/2}. \qquad (8)$$

To determine $T_{\rm eff}$, we compared the observed spectral energy distribution of AR Pav, given by the broad-band photometry to synthetic spectra of cool giants.

For this purpose, first, we summarized the broad-band photometry to match the continuum energy distribution of the giant spectrum. We used the V magnitudes from the total eclipse published by Menzies et al. (1982) and their suggestion for the U and B magnitude of an M III giant of V=12.4. Their measurements in the $I_{\rm C}$ and $R_{\rm C}$ bands of the Cousins system were converted into the Johnson system according to Bessell (1983). Further infrared $JHKL$ photometry was taken from Glass & Webster (1973). Conversion to fluxes was made according to the calibration of Henden & Kaitchuck (1982). The observed fluxes were dereddened with $E_{\rm B-V}$=0.26. Second, we used a grid of models of synthetic spectra for cool giants according to Hauschildt (1999a, 1999b).

To compare the photometric fluxes to the models, we smoothed the calculated spectra with a filter of 50 Å width and a resolution of 25 Å. To scale the modelled spectra to observations we compared the logarithm of the observed and calculated flux with a range of $T_{\rm eff}$. This comparison was performed for wavelength regions of the H,K,L bands with emphasis to the L band, where the model continuum is flat and free of deep absorptions, and thus it should fit best the measured flux (Fig. 7). The V,R,I measurements are affected by absorption features of mainly TiO and VO molecular bands, which become more pronounced at lower temperatures. Therefore the photometric fluxes here are below the level of the continuum. As a result we scaled the synthetic spectra for different $T_{\rm eff}$ to match observations at H,K,L bands and selected those representing the broad-band photometric fluxes in the near-infrared region (see Fig. 7). By this way we were able to determine the effective temperature of the cool component in AR Pav as

$$T_{\rm eff} = 3\,500 \pm 150\,{\rm K}.$$

According to the sensitivity of the near-infrared part of giant's spectra to $T_{\rm eff}$, our comparison method suggests its uncertainty to be of 100 to 200 K (judged by eye). Figure 7 also shows the Planckian function for $T_{\rm eff}$ = 3 500 K scaled to the bolometric flux given by the synthetic spectrum, being of $3.60\times10^{-9}\,{\rm erg\,cm^{-2}\,s^{-1}}$. Having defined the giant's spectrum only through broad-band photometry, there is also an uncertainty in the observed total flux inferred from the range of possible $T_{\rm eff}$. In our case the limiting temperatures of 3 300 and 3 600 K (see Fig. 7) give the range of bolometric fluxes to be $3 - 4\times10^{-9}\,{\rm erg\,cm^{-2}\,s^{-1}}$. So, in accordance with relation (8), the angular radius of the giant component in AR Pav is

$$\theta = (6.5 \pm 1.0)\times 10^{-10},$$

and the distance for the giant's radius of $167\pm15\,{\rm R}_{\odot}$ is thus

$$d = 5.8 \pm 1.5\,{\rm kpc}.$$

The uncertainty represents the maximum range given by possible values of both the stellar and the angular radii. We can verify our bolometric distance through the period-luminosity relation for semiregular variables, the so called Whitelock evolutionary track, in the K-band,

$$M_{\rm K} = -(1.67 \pm 0.12) \log P_{\rm obs} - (3.05 \pm 0.25) \qquad (9)$$

(Bedding & Zijlstra 1998). For the observed period $P_{\rm obs}$ = 106.4 days it gives the bolometric magnitude in the K-band, $M_{\rm K}$ = -6.4±0.5 mag. Then the apparent magnitude $m_{\rm K}$ = 7.2 (Glass & Webster 1973) and the extinction $A_{\rm K}$ = 0.2 mag yield d = 4.9±1.1 kpc.

3.4 Modeling the light curve

3.4.1 The quiescent, 1889–1936, phase

To interpret the quiescent LC of AR Pav as determined by Mayall's data we suggest a model in which the cool component fills its Roche lobe and loses mass into the Roche lobe of the hot component surrounded by a large accretion disk. In the zone where the gas stream impinges on the lateral side of the disk, a hot spot is formed. This region is important for explanation of the minimum profile. To give a successful description of the LC, another active disk region, a bright spot, has to be added (Fig. 8 bottom). Radiation of this region is responsible for the bump of extra light between phases ∼0.4 and ∼0.9. The model does not consider the gas stream radiation. Geometry of these spots is described through their angular dimensions, center longitude and a temperature contrast between the spot and the unperturbed disk edge. In our model we adopted the radial temperature profile of the disk as in models of dwarf novae described by Djurašević (1996). The other essential model elements are explained in detail by Djurašević (1992).

Table 3. Resulting parameters of our modeling of the quiescent photographic LC of AR Pav

Parameter	Value
orbital inclination [°]	87.4 ± 0.2
HC filling coefficient [R_L]	0.192 ± 0.003
HC temperature [K]	28600 ± 700
HC, CC polar radii [A]	0.080, 0.297
CC temperature [K]	(*) 3530
inner and outer disk radii [A]	0.080, 0.444
disk filling coefficient [R_L]	1.00 ± 0.01
disk-edge temperature [K]	12300 ± 230
disk thickness [A]	0.055 ± 0.002
disk temperature coefficient, a_T	0.17 ± 0.14
HS longitude [°]	348 ± 3
HS angular dimensions [°]	10.1 ± 2.1
HS temperature coefficient (=T_{HS}/T_d)	1.42 ± 0.10
BS longitude [°]	255 ± 2
BS angular dimensions [°]	64.5 ± 2.5
BS temperature coefficient (=T_{BS}/T_d)	1.42 ± 0.01
nonsynchronous rotation coefficients	(*) 1.0, 1.0
mass ratio $q = M_{cool}/M_{hot}$	(*) 0.48
HC, CC gravity-darkening coefficients	(*) 0.25, 0.08
HC, CC limb darkening coefficient	0.29, 1.00
limb darkening coefficients of the disk	0.42
$\sum(O-C)^2$ [mag]	1.348

Notes: HC – hot component, CC – cool component, HS – hot spot, BS – bright spot, A – separation between the binary components, R_L – Roche lobe radius, (*) : fixed parameters.

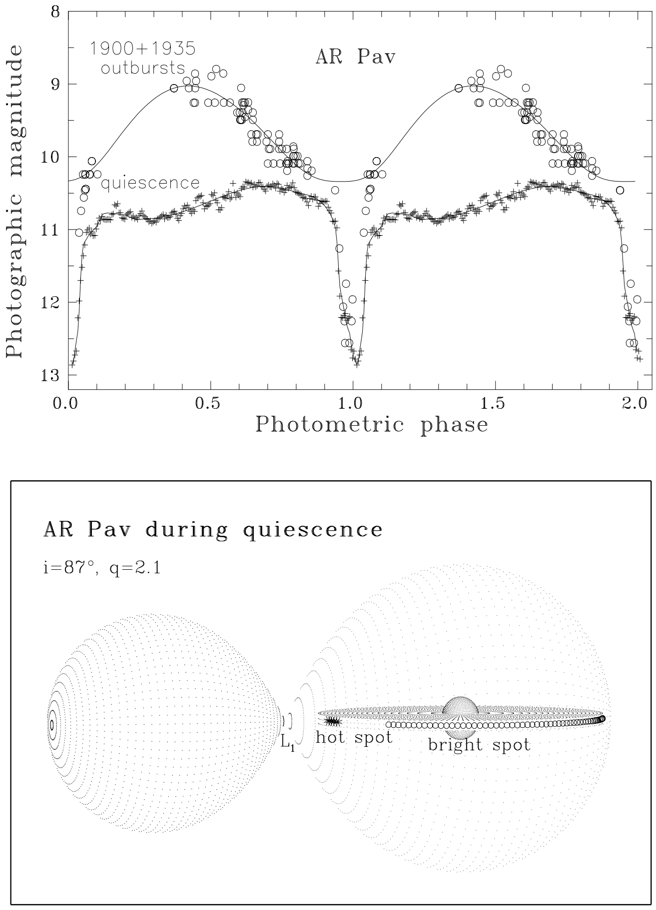

Figure 8. Top: The phase diagram of Mayall's (1937) data. The outburst and quiescent phases are clearly distinguished. Observations are fitted well by our models. Bottom: The Roche model of AR Pav with accretion disk for parameters in Table 3 at the orbital phase 0.80.

The resulting parameters of our analysis are summarized in Table 3, and the corresponding best fit to the data is plotted in the top panel of Fig. 8. It is of interest to note that the best fit corresponds to a larger mass ratio, $q = 0.48$, than that of our analysis in Sect. 3.2. Therefore we performed many trials of fitting the LC for q fixed between 0.3 and 0.4. However, they gave much worse fits with $\sum(O-C)^2 \sim 2-3$ mag. In addition, the accretion disk fills the Roche lobe of the hot component; $R_{\rm disk}^{\rm out} \sim 0.44$ A. The kinetic energy of the mass stream at the impact onto the disk, provided by acceleration from the L_1 point to the disk-edge, cannot be sufficient to produce the observed bump of extra light caused by the bright spot in our model. The same problem exists with the radiation of the hot spot, which is responsible for fitting a standstill in the minimum profile. Thus, in spite the model proposed here offers a good global fit to the observations, it is not able to explain the energetic balance of individual emission regions successfully. It is probable that due to drastic differences in fundamental parameters of symbiotic stars and CVs, the real geometry of accretion disks in symbiotics can differ considerably from that adopted here in analogy with the mass transfer model for CVs (see also Skopal et al. 1998). A theoretical calculation of accretion disk formation in symbiotic binaries should explain better the observed radiation and mass transfer in these extended systems (see e.g. Plavec & Hubený 1994).

3.4.2 Phases of activity

The profile of the LC during the 1900 and 1935 active phases of AR Pav is of the same type as developes during outbursts of AX Per (S94). Therefore, for its explanation, we suggest the model proposed by Skopal (1994). We also observed the expansion of the hot star in AR Pav during these outbursts resulting in the creation of a cool pseudophotosphere (e.g. Andrews 1974), and a mass outflow from the hot star. The latter was indicated by the presence of strong absorption components in hydrogen lines of P-Cygni type just during the 1900 outburst (Mayall 1937). As a result a fraction of material can impact the red giant surface and create a collisional emission region on it. This event causes the wave-like variation in the LC due to differing visibility of this emission region at different orbital phases. Minima and maxima of this extra light occur around orbital phases 0 and 0.5, respectively. However, the exact shape of the LC depends on the location and size of this emission region on the giant star, and on the orbital elements of the binary. We performed a fit to the outburst data by Eq. (6) of Skopal (1994). The resulting best fit is shown in the top panel of Fig. 8. It corresponds to the orbital parameters $e = 0.07 \pm 0.03$, $\omega_{hot} = 2.5 \pm 0.4$ rad and $T_0(phase) = 0.09P_{orb} = 54$ days, which agree well with the orbital solution for radial velocities of the hot component published by Thackeray & Hutchings (1974). However, it is necessary to bear in mind that this interpretation represents only an analogy with AX Per. Its plausibility must be supported independently by spectroscopic observations, which, however, are not available at the present time.

A similar periodic wave-like variation, but more complex in profile and variable during different cycles, developed after 1985.7 (Fig. 1). If we adopt the above mentioned model to match changes in the light maximum during cycles 58 – 65, this infers that the collisional emission region is placed rather on the trailing side of the giant component at the beginning of the activity, while later becomes smaller being located closer to the center of the giant hemisphere facing the hot star. Due to the presence of a large accretion disk around the hot component, an eruption of the central star could have caused a huge reverse mass flow in direction towards the trailing side of the cool giant, and could have changed the shape of the hot object, which could be the reason for the changed timing of the minima after E = 58 (Fig. 5). The reverse mass transfer from the hot to the cool component could have stopped the observed shortening in the orbital period, which became apparent in the $O-C$ diagram after sufficient accumulation of this effect, during epochs E>61.

A more extensive discussion on this out-of-eclipse behaviour is given by Bruch et al. (1994). As the most promising explanation, they suggested that this was caused by a periodic brightening of the accretion disk, resulting from a periodic modulation in the mass transfer due to a semiregular pulsation of the giant star. Recently Djurašević et al. (1998) attempted to fit the LC of AR Pav in outburst in the same way as during quiescence (Sect. 3.4.1). However, they obtained rather unrealistic parameters for the best formal fit. For example, the disk overfills the hot star Roche lobe, and the bright spot has to be located at longitude 165°, i.e. it is best seen at orbital phase ∼0.5. Such a composition of emission regions around the accretor is difficult to understand within a standard canonical model of mass transfer in CVs.

4 CONCLUDING REMARKS

We have presented and analysed historical, 1889 – 1998, photometric observations of the symbiotic binary AR Pav and our conclusions may be summarized as follows:

(i) The observed mid-points of eclipses in the quiescent LC from the beginning of observations (1889) to the orbital cycle 58 (1985.7), revealed a quadratic trend in the $O-C$ residuals. The calculated quadratic ephemeris corresponds to an initial period of 605.18 days and a rate of change of the orbital period $\dot{P} = -3.5 \pm 0.8 \times 10^{-5}$. During this period the mass is transferred from the less to the more massive star. This indicates a slow mass and angular momentum loss from the accretor. During the active stage, from E = 59 on, the $O-C$ residuals do not obey the quadratic ephemeris. This is caused mainly by changes in the shape of the eclipsed object. We interpret these variation by an eruption of the hot star.

(ii) Evolution in profiles of the measured eclipses indicates a strong variability of the eclipsed object during active phases, while during quiescence it is relatively stable, having a radius of $\sim 0.1A$. Variation of the red giant radius is supported by about 106-day periodic light fluctuations in the visual data.

(iii) We determined the distance to the system to be 5.8±1.5 kpc, the mass ratio of the giant to the hot star, $M_{\rm g}/M_{\rm h} = 0.4 \pm 0.1$, the mass of the giant, $M_{\rm g} = 1.8 + 1/-0.5\,{\rm M}_{\odot}$ and its radius, $R_{\rm g} = 167 \pm 15\,{\rm R}_{\odot}$.

(iv) During quiescence, the LC has characteristic features similar to those observed in CVs. It can be formally reproduced by a model of a large accretion disk around the hot component. However, our model is not able to explain the energy balance of main emission components in the system. This suggests a different geometry of the transferred material in the Roche lobe of the accretor in symbiotic binaries compared with that of CVs.

(v) During active phases the profile of the LC changes considerably. A complex wave-like variation developed as a function of orbital phase at ∼1 mag level. This behaviour is discussed in the frame of a model of a collisionally heated emission region located on the giant surface due to the hot star eruption. However, plausibility of this interpretation must be confirmed by spectroscopic observations.

ACKNOWLEDGMENTS

This research has been supported through the Alexander von Humboldt foundation, the NATO collaborative grant No. 960332 and by Ministry for Sciences and Technology of Serbia through the project "Astrometrical, Astrodynamical and Astrophysical investigations". AS acknowledges the hospitality of the Astronomical Institute, University of Erlangen-Nürnberg, in Bamberg.

REFERENCES

Andrews, P.J., 1974, MNRAS, 167, 635
Batten A.H., 1973, *Binary and Multiple Systems of Stars*, Pergamon press, Oxford, p. 83
Bedding T.R., Zijlstra A.A., 1998, ApJ, 506, L47
Bessell M.S., 1983, PASP, 95, 480
Bruch A., Niehues M., Jones A.F., 1994, A&A, 287, 829
Djurašević G., 1992, Ap&SS, 196, 267
Djurašević G., 1996, Ap&SS, submitted
Djurašević G., Skopal A., Jones A., Rovithis-Livaniou H., Rovithis P., 1998, in: J. Dušek & M. Zejda (eds.), 'Proceedings of the 2.th Conference on Variable Star Research', N. Copernicus Observatory, Brno, p. 82
Eggleton P.P., 1983, ApJ, 268, 368
Ghedini S., 1982, *Software for Photometric Astronomy*, Willmann-Bell, Inc. Publ. Comp., Richmond
Glass I.S., Webster B.L., 1973, MNRAS, 165, 77
Hauschildt P.H., 1999a (private communication)
Hauschildt P.H., 1999b, ApJ, (in press)
Henden A.A., Kaitchuck R.H., 1982, *Astronomical Photometry*, Van Nostrand Reinhold Company, New York, p. 50
Hutchings J.B., Cowley A.P., Ake T.B., Imhoff C.L., 1983, ApJ, 275, 271
Kenyon S.J., Webbink R.F., 1984, ApJ, 279, 252
Kohoutek L., 1999 (private communication)
Mayall M. W., 1937, Harvard Ann., 105, 491
Menzies J.W., Coulson I.M., Caldwell J.R.A., Corben P.M., 1982, MNRAS, 200, 463
Ostlie D., Cox A.N., 1986, ApJ, 311, 864
Plavec M.J., Hubený I., 1994, in: A. Shafter (ed.), 'Interacting Binary Stars', ASP Conf. Ser. 56, p. 87
Schulte-Ladbeck R.E., 1988, A&A, 189, 97
Skopal A., 1994, A&A, 286, 453 (S94)
Skopal A., 1998, A&A, 338, 599
Skopal A., Bode M.F., Lloyd H.M., Drechsel H., 1998, A&A, 331, 179
Thackeray A.D., 1959, MNRAS, 119, 629
Thackeray A.D., Hutchings J.B., 1974, MNRAS, 167, 319